**Article:**
Hettmanczyk, L., Spall, S.J.P., Klenk, S. et al. (4 more authors) (2017) Structural, Electrochemical, and Photochemical Properties of Mono- and Digold(I) Complexes Containing Mesoionic Carbenes. European Journal of Inorganic Chemistry, 2017 (14). pp. 2112-2121. ISSN 1434-1948

https://doi.org/10.1002/ejic.201700056

# Structural, Electrochemical and Photochemical Properties of Mono and Digold(I) Complexes Containing Mesoionic Carbenes

Lara Hettmanczyk,[a] Steven J. P. Spall,[b] Sinja Klenk,[a] Margarethe van der Meer,[a] Stephan Hohloch,[a] Julia A. Weinstein,[b] Biprajit Sarkar*[a]

**Keywords**: Gold/Triazolylidene/Electrochemistry/Mesoionic Carbene/Emission

[a]Institut für Chemie und Biochemie, Anorganische Chemie, Freie Universität Berlin, Fabeckstraße 34-36, D-14195, Berlin, Germany

E-mail: biprajit.sarkar@fu-berlin.de

Homepage:
http://www.bcp.fuberlin.de/en/chemie/chemie/forschung/InorgChem/agsarkar/index.html

[b]Department of Chemistry, University of Sheffield, Sheffield, S3 7HF (UK)

💻 Supporting information for this article is available on the WWW under or from the authors.

**Abstract**

Triazolylidenes are a prominent class of mesoionic carbenes (MICs) that are currently widely used in organometallic chemistry. Usually metal complexes of such ligands are used as homogeneous catalysts even though they have a vast potential in other branches of chemistry. We present here three related gold(I) complexes with MIC ligands: a neutral mononuclear chlorido complex [AuCl(MIC)], a cationic mononuclear complex containing two MIC ligands $[Au(MIC)_2]BF_4$ and a dicationic digold(I) complex containing two di-MIC ligands $[Au_2(\kappa^1, \kappa^1, \mu\text{-di-MIC})_2](BF_4)_2$. The complexes were characterized by $^1H$ and $^{13}C\{^1H\}$ NMR spectroscopy, mass spectrometry and single crystal X-ray diffraction. The gold(I) centers are linearly coordinated through either one MIC-*C* and chlorido donors or through two MIC-*C* donors. The triazolylidenes display a delocalized bonding situation within the ring. Additionally, a short Au-Au distance of about 3 Å is observed for the digold(I) complex. All complexes display reduction steps in their cyclic voltammograms and these are assigned to the reduction of the MIC ligands, as opposed to the generation of gold(0). The complexes emit in the range ~500 nm, with the lifetimes of several microseconds in deoxygenated solutions; the emission intensity and lifetime are strongly decreased by the presence of oxygen, supporting the triplet origin of the emissive state. The present results display the utility of MIC ligands for generating electro and photoactive molecules.

## Introduction

Mesoionic carbene (MIC) ligands are currently extremely popular in organometallic chemistry. Apart from comparisons with their "normal" N-heterocyclic carbene (NHC) ligands, other obvious reasons for their popularity are their unusual bonding situation and their strong donor properties.[1] 1,2,3-triazol-5-ylidenes are arguably currently the most prominent class of MIC ligands.[1-2] Reasons for this popularity are, among others, their facile and modular synthesis through the copper(I) catalyzed azide-alkyne cycloaddition reaction.[3] Thus, a variety of transition metal complexes, particularly with late transition metals, have been reported with these ligands.[2] A survey of these metal complexes shows that apart from synthesis and characterization of the metal complexes, an overwhelming majority of these work deals with the utility of the corresponding metal complexes in homogeneous catalysis.[1,2,4] This fact is perhaps not surprising considering the huge popularity of metal complexes of NHC ligands in homogeneous catalysis. However, MIC ligands of the triazolylidene type are potentially interesting for a host of other branches like supramolecular chemistry, photochemistry and unusual bond activation reactions.[5,6] Thus, it was shown early on in the development of such ligands that their ruthenium(II) complexes display excellent photochemical and electrochemical properties.[6a,b] More recent studies have shown the utility of these ligands in photochemical studies with metal centers such as iron(II), iridium(III) and platinum(II).[6c-e] In some of the aforementioned cases, unprecedented lifetimes of the excited states were obtained by using MIC ligands.

In keeping with our interest in electrochemical and photochemical properties of transition metal complexes, we have recently shown that cobalt(III) complexes containing MIC ligands are potent catalysts for electrochemical dihydrogen production, displaying the lowest known over-potential till date.[7a] Furthermore, we have also shown that gold(I) complexes containing redox-active MIC ligands are capable of performing electron transfer induced catalysis[7b,7c] and that redox-rich systems can be built with palladium(II) complexes of MIC ligands[7d]. Herein we present the synthesis and complete characterization of the gold(I) complexes **1**, **[2]BF$_4$** and **[3](BF$_4$)$_2$** (Scheme 1). Apart from results from NMR spectroscopy and single crystal X-ray diffraction, the main focus of this work is on the electrochemical and photochemical properties of the three complexes. We show below the effect of one versus two MIC ligands, and one versus two gold(I) centers on the electrochemical and photochemical properties of the complexes. In doing so, we try to address the issues of redox processes on the MIC ligands versus the gold(I) centers, and provide insights into the nature of the excited states in these complexes. Even though several gold(I) complexes with triazolylidene type MIC

ligands have been reported in the literature, to the best of our knowledge the electrochemical and photochemical properties of such complexes have never been investigated before.[4f, 5g, 8,10] It should be mentioned here that gold(I) complexes with NHC ligands are known to display intriguing photochemical properties.[5c,9] Below we present results from synthesis, NMR spectroscopy, single crystal X-ray diffraction, electrochemistry, emission spectroscopy and DFT calculations to address the issues mentioned above.

## Results and Discussion

### Synthesis and Crystal Structures

The mono and bitriazolium salts **[L1]I** and **[L2](BF$_4$)$_2$** that are the precursors to the MIC ligands were synthesized according to reported synthetic routes. The chlorido complex **1**, which has been reported elsewhere,[10] was synthesized through the transmetallation route by using **[L1]I**, $Ag_2O$ and [AuCl($SMe_2$)]. **1** was re-synthesized for the present work for the investigation of its electrochemical and photochemical properties.[10] Reaction of complex **1** with $AgBF_4$ led to the formation of the cationic mononuclear gold(I) complex **[2]BF$_4$** that contains two monodentate MIC ligands (Scheme 1 and experimental section). The yield of this complex was 80 % with respect to the ligand (40 % with respect to gold). The digold(I) complex **[3](BF$_4$)$_2$** was synthesized, like complex **1**, through the transmetallation route by using $Ag_2O$ and [AuCl($SMe_2$)].

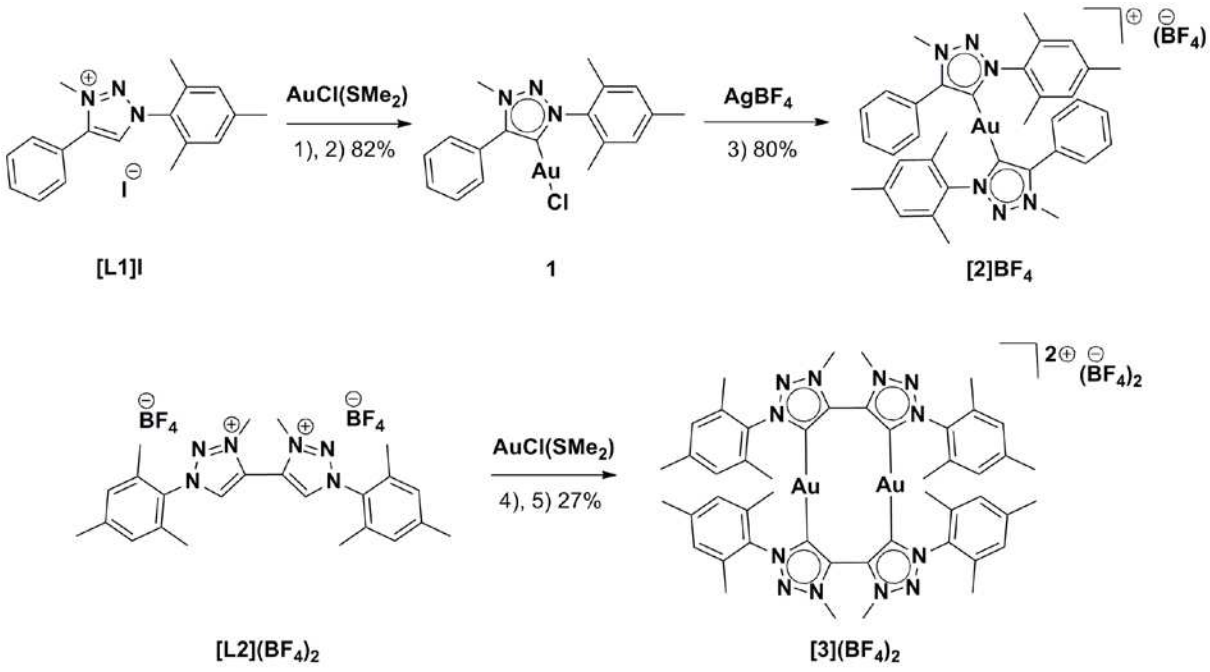


Scheme 1. Synthesis of the complexes **1**–**3**. Complex **1**: 1) $Ag_2O$, $CH_2Cl_2$, room temperature; 2) AuCl($SMe_2$), $CH_2Cl_2$, room temperature; Complex **[2]BF$_4$**: 3) $AgBF_4$, $CH_2Cl_2$, room temperature; 4)

$Ag_2O$, $CH_3CN$, 50°C; Complex **[3](BF$_4$)$_2$** 5) $AuCl(SMe_2)$, $CH_3CN$, room temperature. Complex **1** was previously reported and was re-synthesized here for the investigation of its electrochemical and photochemical properties.[10]

The absence of the proton signals corresponding to the C-H protons of the triazolium rings in the $^1$H NMR spectra of all complexes provided a first indication for the formation of the triazolylidene complexes (Figure S1–S3). ESI-MS spectra of the complexes showed peaks corresponding to the sodium salt of **1**, and the cationic parts for **[2]BF$_4$** and **[3](BF$_4$)$_2$** (experimental section). In the $^{13}C\{^1H\}$ NMR spectra of these complexes the MIC-*C* was observed at 160.6, 174.3 and 176.4 ppm for **1**, **[2]BF$_4$** and **[3](BF$_4$)$_2$** respectively (Figure S1–S3). These data show the downfield shift of the MIC-*C* on replacing a chlorido ligand with a second MIC ligand. Single crystal diffraction data on complex **1** were reported elsewhere and we will briefly discuss the bond lengths and bond angles here for comparison purposes.[10] **[2]BF$_4$** was crystallized by condensation of hexane into a dichloromethane solution at ambient temperatures, and **[3](BF$_4$)$_2$** by slow condensation of diethylether into acetonitrile at 8 °C. **[2]BF$_4$** crystallizes in the monoclinic $P2_1/c$ and **[3](BF$_4$)$_2$** in the triclinic *P*-1 space group (Table S3). In **[2]BF$_4$** the gold center is linearly coordinated by two *C*-donors from two different monodentate MIC ligands (Figure 1). The Au-C1 and Au1-C1A distance to the two MIC donors are 2.014(8) and 2.005(8) Å respectively. Both these Au-C bond lengths in **[2]BF$_4$** are longer than the Au-C bond length of 1.973(1) observed for **1**. This effect is likely related the stronger *trans* influence of the MIC ligands even though steric effects in **[2]BF$_4$** cannot be completely ruled out. The intra-ring bond lengths inside the triazolylidene rings point to a delocalized bonding situation within those rings (Table 1). The C2-C1-N3 and the C2A-C1A-N3A angles at the carbene carbon center are 101.6(7) and 102(6)° respectively. The C1-Au1-C1A angle is 178.3(3)° displaying the near perfect linear coordination at the gold(I) center. The aryl substituents are all twisted with respect to the triazolylidene rings with dihedral angles between 48 and 75° (Table S5).

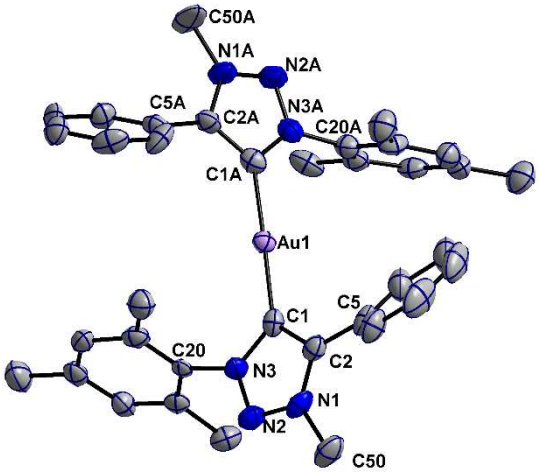


Figure 1. ORTEP diagram of **[2]BF$_4$**. Ellipsoids are drawn at 50 % probability. Hydrogen atoms and counter ions are omitted for clarity.

Table 1. Selected measured bond length in Å of complexes **1**,[a] **[2](BF$_4$)** and **[3](BF$_4$)$_2$**

| | **1**[a] | **[2](BF$_4$)** | **[3](BF$_4$)$_2$** |
|---|---|---|---|
| C1 - C2 | 1.394(11) | 1.381(11) | 1.394(7) |
| C1A - C2A | - | 1.389(11) | 1.386(7) |
| C3 - C4 | - | - | 1.384(7) |
| C3A - C4A | - | - | 1.392(6) |
| C1 - N3 | 1.384(10) | 1.374(9) | 1.359(7) |
| C1A - N3A | - | 1.378(10) | 1.363(6) |
| C3 - N6 | - | - | 1.355(6) |
| C3A - N6A | - | - | 1.369(6) |
| C2 - N1 | 1.360(10) | | 1.359(7) |
| C2A - N1A | - | 1.359(10) | 1.365(6) |
| C4 - N4 | - | - | 1.367(7) |
| C4A - N4A | - | - | 1.358(6) |
| N1 - N2 | 1.316(9) | 1.312(9) | 1.312(7) |
| N1A - N2A | - | 1.323(9) | 1.310(6) |
| N4 - N5 | - | - | 1.302(7) |
| N4A - N5A | - | - | 1.317(5) |
| N2 - N3 | 1.342(8) | 1.324(8) | 1.330(6) |
| N2A - N3A | - | 1.336(9) | 1.331(6) |
| N5 - N6 | - | - | 1.333(6) |
| N5A - N6A | - | - | 1.336(5) |
| C2 - C5 | 1.478(11) | 1.743(12) | - |
| C2A - C5A | - | 1.466(10) | - |
| N3 - C20 | 1.439(10) | 1.443(9) | 1.452(7) |
| N3A - C20A | - | 1.446(19) | 1.446(6) |
| N6 - C35 | - | - | 1.447(7) |

| | | | |
|---|---|---|---|
| N6A - C35A | - | - | 1.446(6) |
| N1 - C50 | 1.462(10) | 1.446(10) | 1.475(7) |
| N1 - C50A | - | 1.475(10) | 1.460(7) |
| N4 - C51 | - | - | 1.442(7) |
| N4A - C51A | - | - | 1.463(6) |
| Au1 - C1 | 1.973(1) | 2.014(8) | 2.010(5) |
| Au1 - C1A | - | 2.005(8) | 2.018(4) |
| Au2 - C3 | - | - | 2.019(4) |
| Au2 - C3A | - | - | 2.007(4) |
| Au1 - Au2 | - | - | 2.996(8) |
| Au1 - Cl1 | 2.281(2) | - | - |

[a] From reference [10]

A look at the molecular structure of **[3](BF$_4$)$_2$** in crystal shows the $\kappa^1$, $\kappa^1$, $\mu$-bridging mode of the two ditriazolylidene ligands leading to the formation of a digold complex (Figure 2). The gold centers in **[3](BF$_4$)$_2$** are coordinated to a MIC-*C* from each of the triazolylidene ligands. The Au-C(MIC) distances are in the same range as discussed for **[2]BF$_4$** above (Table 1). The bonding situation inside all four triazolylidene rings in the dinuclear complex is delocalized (Table S4). The angles at the MIC-C atoms are between 101.7(4)-102.8(4)° (Table S4). The C1-Au-C1A and the C3-Au2-C3A angles are 176.1(1) and 177.7(1)° respectively showing the near linear coordination geometry at the gold centers. All the peripheral aryl substituents are twisted with respect to the triazolylidene rings to which they are connected with dihedral angles close to 70° (Table S5). The two triazolylidene rings within both the ditriazolylidene ligand are also twisted with respect to each other with dihedral angles of 44.9(3) and 47.7(2)°. This twisting is possibly necessary to avoid steric hindrance between the adjacent methyl groups attached to the nitrogen atoms of the two connected triazolylidene rings. The intramolecular Au1-Au2 distance in **[3](BF$_4$)$_2$** is 2.996(8) Å and is clearly shorter than the sum of the van der Waals radius of the two gold centers.[11] While it is tempting to take this short Au-Au distance as a sign of aurophilic interactions, it should be mentioned that the $\kappa^1$, $\kappa^1$, $\mu$-bridging mode of the two di-MIC ligands actually forces the gold centers to approach each other.

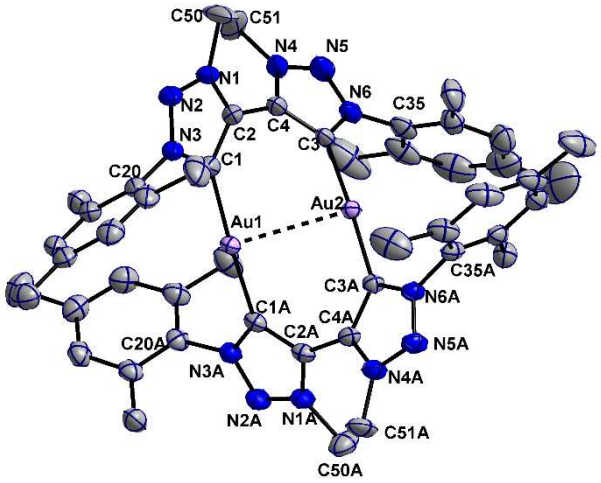


Figure 2. ORTEP diagram of **[3](BF$_4$)$_2$**. Ellipsoids are drawn at 50 % probability. Hydrogen atoms, counter ions and solvent molecules are omitted for clarity.

**Electrochemistry**

The triazolium ion **[L1]$^+$** displays an one-electron reduction wave in THF / 0.1 M $Bu_4NPF_6$ with an $E_{pc}$ of -1.89 V. **[L1]BF$_4$** was used instead of **[L1]I** for cyclic voltammetric measurements due to additional overlaying redox processes of the $I^-$. Even though a reverse wave is observed on the re-oxidation cycle at -1.75 V (Figure 3), the peak current ratio of the forward and the reverse scans is less than one, pointing to only a quasi-reversible one-electron reduction step. In analogy with the reductive response of 1,2,3-triazoles reported earlier, we assign this reduction wave to the reduction of the triazolium ring in **[L1]$^+$**.[7b] No oxidation wave was observed within the solvent potential window. The bitriazolium ion **[L2]$^{2+}$** displays two one-electron reduction waves with $E_{pc}$ at -1.82 and -2.05 V (Figure 3). Small re-oxidation waves coupled to the two reduction waves are seen at -1.71 and -1.87 V. Additionally, two other re-oxidation waves that are a follow-up of the reduction waves are observed at large positively shifted potentials of -0.91 and -0.55 V (Figure 3). The lack of overall reversibility of the reduction steps precluded us from gathering independent spectroelectrochemical data on the redox processes. However, the nature of the cyclic voltammograms strongly point towards the operation of an electron transfer-chemical reaction (EC) or a more complex kind of mechanism. In analogy to **[L1]$^+$**, we assign the two reduction steps to the successive reduction of the two triazolium ions in **[L2]$^{2+}$**. The first reduction potential of **[L2]$^{2+}$** is almost identical to the reduction potential of **[L1]$^+$**. These data suggest that the higher charge of the bitriazolium ion is likely compensated through electronic effects related to the incorporation of the second triazolium unit with a different substitution pattern in **[L2]$^{2+}$** as compared to **[L1]$^+$**. Additionally, the observation of a second reduction step at a different potential for the

symmetrically substituted ditriazolium ion **[L2]**$^{2+}$ suggests the operation of possible electronic coupling between the two connected triazolium units.

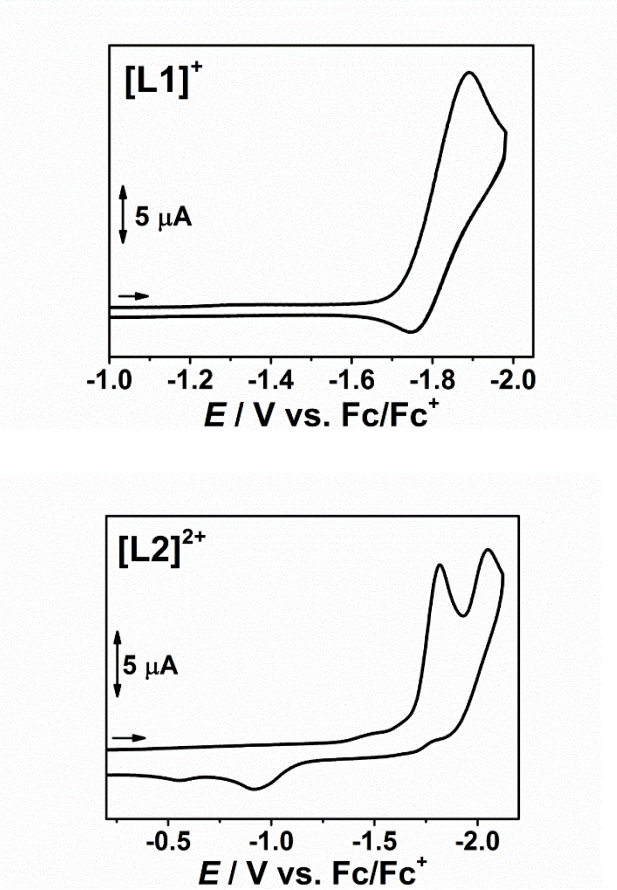


Figure 3. Cyclic voltammograms of **[L1]**$^{+}$ (top) and **[L2]**$^{2+}$ (bottom) in THF / 0.1 M $Bu_4NPF_6$ at room temperature. $Fc/Fc^{+}$ was used as internal standard.

The chlorido gold(I) complex **1** displays an one-electron reduction wave at -2.52 V at room temperature (Figure 4). At room temperature no re-oxidation wave corresponding to the reduction wave was observed for this complex. However, on cooling the sample to -40 °C a re-oxidation wave appears at -2.39 V (Figure 4) suggesting the quasi-reversible nature of the reduction step. It is seen that on converting the cationic triazolium ion **[L1]**$^{+}$ to the corresponding neutral MIC-Au-chlorido complex, the reduction step is negatively shifted by about 600 mV. This negative shift is likely a result of the change in charge (cationic versus neutral) as well as the incorporation of the electron withdrawing chloride ligand in **1**. In comparison to the free triazolium salt, we assign this reduction step to the reduction of the triazolylidene unit in complex **1**.

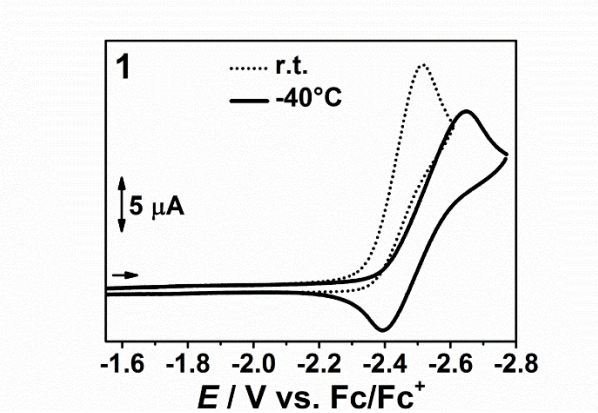


Figure 4. Cyclic voltammograms of **1** in THF / 0.1 M $Bu_4NPF_6$ at room temperature and at -40 °C. $Fc/Fc^+$ was used as internal standard.

The complex $\mathbf{[2]^+}$ displays three reduction waves at -2.55, -2.73 and -2.83 V at room temperature. Cooling the sample down to -30 °C resulted in the observance of only two reduction waves, the second of which is rather broad, possibly indicating an overlap of the latter two waves observed at room temperature (Figure S5–S6). The reversibility of the cyclic voltammogram improves at -40 °C with re-oxidation peaks coupled to the reduction peaks appearing at -2.33 and -2.56 V. Additionally, a large positively shifted re-oxidation wave is seen at -0.87 V. The potential of the first reduction is very similar for **1** and $\mathbf{[2]^+}$. This fact indicates that on moving from **1** to $\mathbf{[2]^+}$, the increase in the positive charge is compensated by the substitution of an electronic withdrawing chlorido ligand with a strongly donating MIC.

The digold complex $\mathbf{[3]^{2+}}$ displays two reduction waves at -2.0 and -2.20 V at room temperature. Small re-oxidation peaks corresponding to these reduction peaks are observed at -1.88 and -2.05 V respectively (Figure 5). Lowering the temperature did not lead to any significant changes in the cyclic voltammogram of this complex (Figure S7). A comparison with the bitriazolium ion $\mathbf{[L2]^{2+}}$ and the cationic monogold(I) complex $\mathbf{[2]^+}$, both of which display two relatively well separated one-electron reduction waves, would lead one to conclude that $\mathbf{[3]^{2+}}$ should display four reduction waves. Apart from the two reduction waves shown in Figure 5, no other reduction processes are observed for complex $\mathbf{[3]^{2+}}$ within the solvent window. Unfortunately, the use of the Baranski method for the determination of number of electrons that flow during a redox process proved to be inconclusive for complex $\mathbf{[3]^{2+}}$. Hence, we are not in a position to comment if we indeed observe two two-electron waves, or if the other two reduction waves actually fall outside the solvent potential window. A comparison with the electrochemical response of $\mathbf{[L2]^{2+}}$ and $\mathbf{[2]^+}$ would led one to conclude on the two-electron nature of the redox waves in $\mathbf{[3]^{2+}}$. However, we do not have any conclusive proof for

this fact as yet. The complexes **1**, **[2]**$^{+}$ and **[3]**$^{2+}$ did not display any oxidation waves within the solvent potential window.

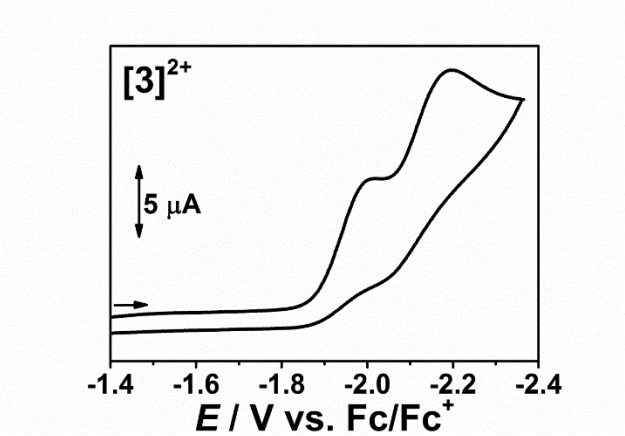


Figure 5. Cyclic voltammogram of **[3]**$^{2+}$ in THF / 0.1 M $Bu_4NPF_6$ at room temperature. $Fc/Fc^{+}$ was used as internal standard.

Spin density calculations were carried out to provide indirect insights into the locus of reduction in the studied complexes. A look at the Löwdin spin population distribution obtained from structure based DFT calculations provide values of 96 %, 85 % and 100 % spin population on one or both of the triazolylidene complexes for the reduced forms **[1]**$^{-\bullet}$, **[2]**$^{\bullet}$ and **[3]**$^{+\bullet}$ respectively (Figure 6). Additionally, the LUMO's of **1**, **[2]**$^{+}$ and **[3]**$^{2+}$ are all completely localized on the triazolylidene ligands (see discussion on TD-DFT below).

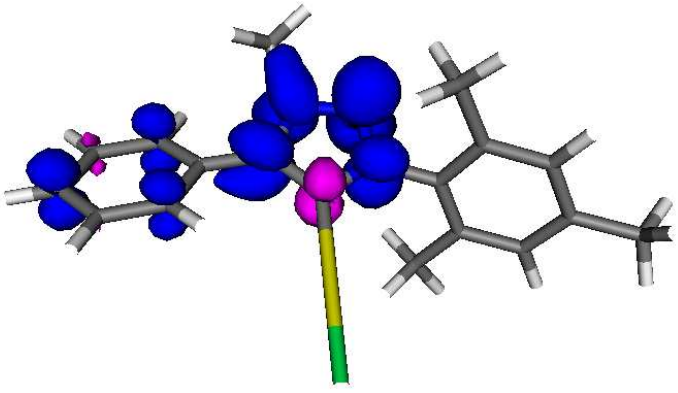

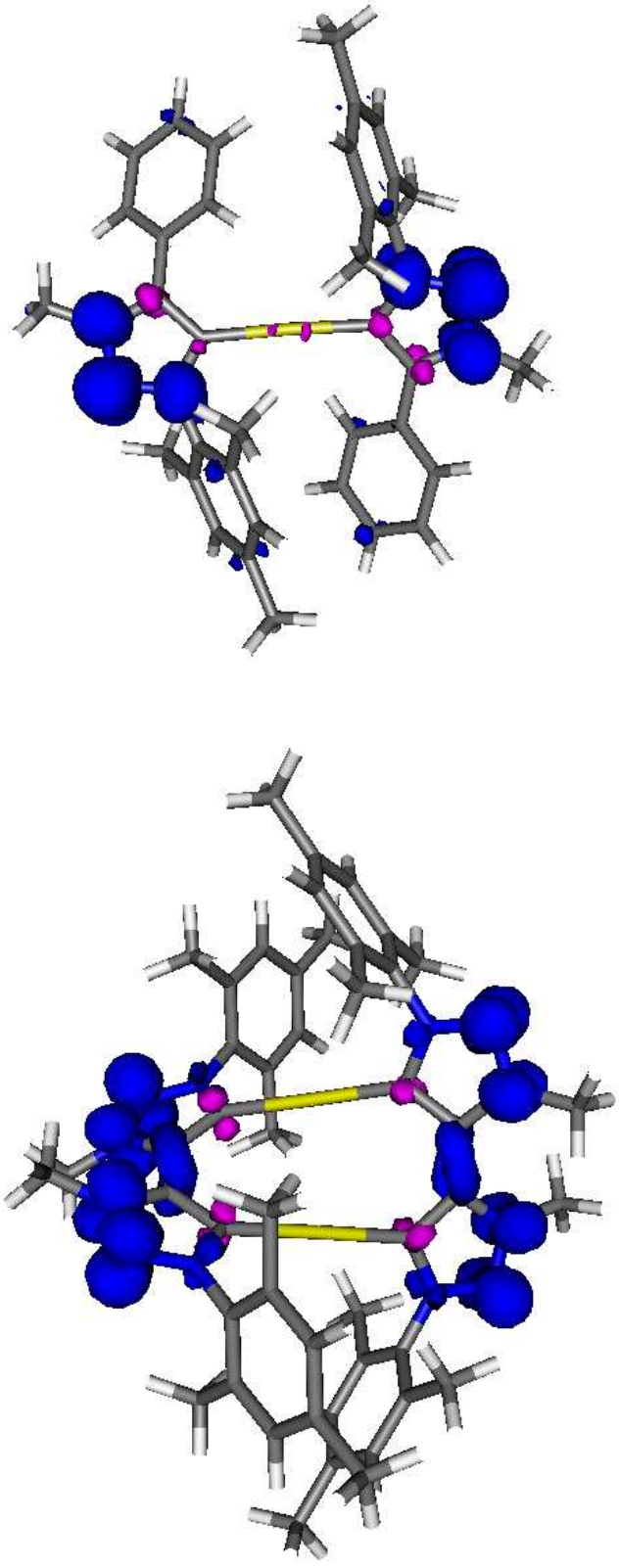

Figure 6. Löwdin spin population distribution for the one-electron reduced complexes **[1]**$^{-\bullet}$ (top), **[2]**$^{\bullet}$ (middle) and **[3]**$^{+\bullet}$ (bottom).

Thus, the comparison of the electrochemical properties of the triazolium salts with the gold complexes, as well as a look at the spin population plot for the one-electron reduced forms of all complexes clearly show that reduction in these complexes occur at the triazolylidene ligands. Such reduction steps lead to the formation of a $d^{10}$ closed-shell gold(I) center with bound triazolylidene radicals. Thus, the formulation of the reduced forms of these gold complexes with MIC ligands are different from what has been recently reported for the reduced forms of gold and copper complexes with cyclic alkyl amino carbenes (CAAC).[12] In those cases, the reduced forms were formulated as gold(0) or copper(0) centers bound to neutral CAAC ligand which is a result of the gold(I) or copper(I) centers in those complexes getting reduced as opposed to the carbene ligands.

**UV-vis Spectroscopy, TD-DFT Calculations and Emission Properties**

All three complexes display relatively similar features in their UV-vis spectra. The main, broad absorption bands are centered around 240-300 nm, whilst complex **[3](BF$_4$)$_2$** also exhibits a shoulder tailing to 340 nm (Figure 7).

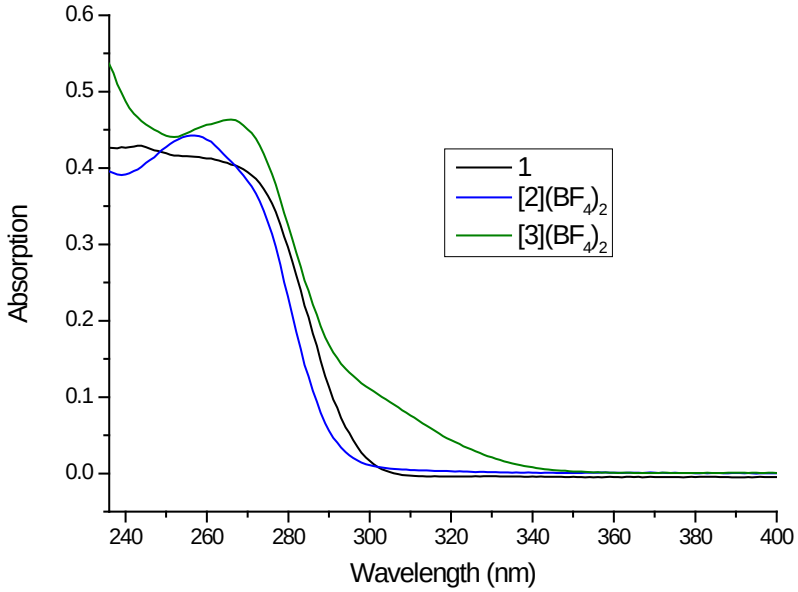


Figure 7. UV/Vis spectra of gold complexes studied, in DCM.

TD-DFT calculations were carried out to get insights into the origin of the aforementioned absorption bands. The results for **[2](BF$_4$)** are discussed here whereas those for **1** and **[3](BF$_4$)$_2$** are shown in Tables S2-S3 and Figures S9-S10 in the supporting information. For the band in **[2](BF$_4$)** which is centered around 260 nm, TD-DFT shows the main contributions to be from HOMO -8 → LUMO +1, HOMO -8 → LUMO and HOMO -7 →

LUMO (Figure 8, Table 2). Even though the values of the energies of these transitions obtained from the calculations should be taken with caution, they deliver what one would intuitively expect for such gold(I) complexes. These broad bands can thus be best described as a mixture of metal to ligand charge transfer (MLCT) from the gold(I) centers to the triazolylidene ligands and intraligand π-π* transitions within the triazolylidene ligands.

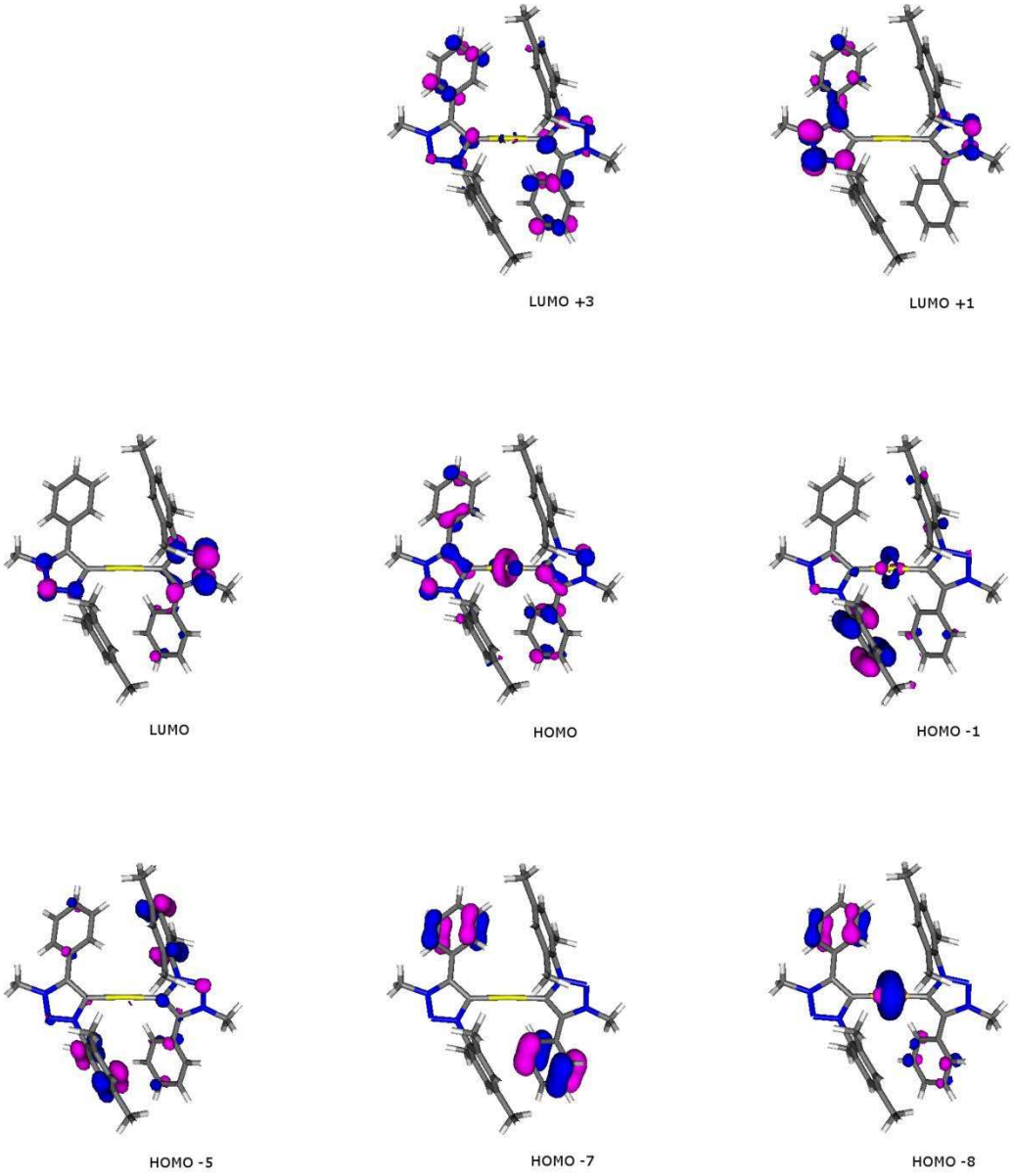


Figure 8. Calculated frontier orbitals of **[2](BF$_4$)**.

Table 2. UV-vis data of **[2](BF$_4$)** together with TD-DFT calculated transitions.

| | Main contributing excitation (%) | Transition energy (nm) | Oscillator strength | Exp. Transition energy (nm) | Molar absorption coefficient ($M^{-1}$ $cm^{-1}$) |
|---|---|---|---|---|---|
| **[2]$^+$** | | | | | |
| | HOMO -5 → LUMO +3 (21) | 224 | 0.040 | | |
| | HOMO -8 → LUMO +1 (35) | 260 | 0.038 | 255 | 26287 |
| | HOMO -8 → LUMO (31)<br>HOMO -7 → LUMO (16) | 263 | 0.035 | 268 | 22387 sh |
| | HOMO -1 → LUMO (36)<br>HOMO -1 → LUMO +1 (24)<br>HOMO → LUMO (18) | 319 | 0.003 | 324 | 736 sh |

In aerated dichloromethane all of the complexes show an intense emission band with ca. 500-nm maximum (Figure 9), for which excitation spectra coincide with the absorption spectra (See figure S8, SI). The intensity of the 500 nm emission is enhanced greatly upon deoxygenating of the solutions. The emission at 500 nm has the lifetime of several microseconds (Table 3) in aerated solution, which is further increased upon removal of oxygen. We therefore assign the 500 nm band to phosphorescence, occurring from a lowest triplet state. Complexes **1** and **[2](BF$_4$)$_2$** also exhibited very weak emission at 320 nm and 350 nm, respectively which was unaffected by the presence of oxygen in solution, and is therefore assigned as fluorescence (it must be noted that the intensity of the emission was too low to reliably record excitation spectra). Che et al. have reported similar complexes with two emission bands centred at ca. 450 nm and ca. 625 nm assigned to prompt fluorescence and phosphorescence respectively, in these complexes only the phosphorescence band exhibited sensitivity towards the presence of oxygen.[9j]

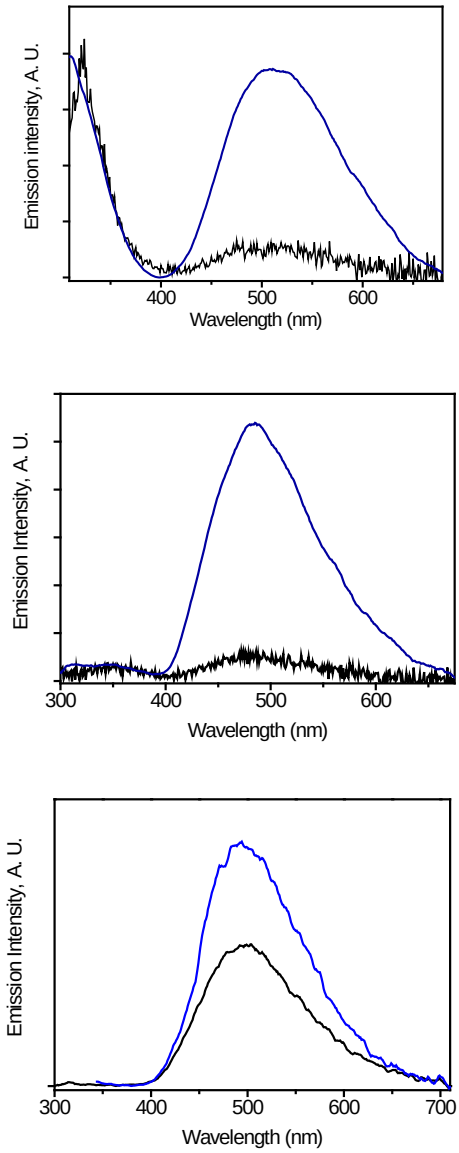


Figure 9. Emission spectra of complexes in DCM with 270 nm excitation wavelength, emission spectra were recorded at 270 – 450 nm with no filter and 450 – 800 nm using a filter with transmission >370 nm (Blue: deoxygenated, black: oxygenated).

Table 3. Photophysical data for the complexes, recorded in $CH_2Cl_2$ solutions at r.t. Lifetime measurements performed with 270 nm, 750- ps excitation .

| **Compound** | **Conditions** | **Absorption $\lambda_{max}$ [nm]** | **Main Emission $\lambda_{max}$ [nm]** | **Lifetime / µs** |
|---|---|---|---|---|

| | | | | |
|---|---|---|---|---|
| **1** | Aerated | 243 | 514 | 1.9 ± 0.1 |
| **1** | Deoxygenated | 243 | 514 | 4.2 ± 0.2 |
| **[2]BF$_4$** | Aerated | 256 | 483 | 2.5 ± 0.2 |
| **[2]BF$_4$** | Deoxygenated | 256 | 483 | 6.2 ± 0.3 |
| **[3](BF$_4$)$_2$** | Aerated | 266 | 495 | 1.6 ± 0.1 |
| **[3](BF$_4$)$_2$** | Deoxygenated | 266 | 495 | 2.1 ± 0.1 |

## Conclusion

In conclusion, we have presented here the synthesis and complete characterization of two related cationic gold(I) complexes with mesonic carbene (MIC) ligands. The new complexes [Au(MIC)$_2$]BF$_4$ (**[2]BF$_4$**) and [Au$_2$($\kappa^1$,$\kappa^1$,$\mu$-di-MIC)$_2$](BF$_4$)$_2$ (**[3](BF$_4$)$_2$**) were characterized by $^1$H and $^{13}$C{$^1$H} NMR spectroscopy and with single crystal X-ray diffraction studies. The gold(I) centers in both complexes are linearly coordinated with two MIC-C donors. The digold(I) complex **[3](BF$_4$)$_2$** displays a short intramolecular Au-Au distance of 2.999 Å. The complexes **[2](BF$_4$)** and **[3](BF$_4$)$_2$** were compared with the reported complex [AuCl(MIC)] (**1**) in terms of their electrochemical and photochemical properties. All complexes display one or more reduction steps in their cyclic voltammogram. A comparison of these electrochemical data with those of the corresponding free triazolium salts shows the reduction of the MIC ligands in these complexes. This observation is in contrast to what has been observed for coinage metal complexes of cyclic alkyl amino carbenes where metal centered reductions were proposed.[12] The complexes display strong absorption bands around 260-270 nm which can be assigned with the help of TD-DFT calculations to a mixture of intraligand π-π* transition and MLCT

transition. The photophysical properties of the compounds indicate presence of two excited states, a singlet state from which weak fluorescence emanates; and a triplet state which is characterized by relatively intense and long-lived phosphorescence. We have shown here that the MIC ligands of triazolylidene type are valuable components for photo and electro active molecules. Thus, apart from a wide range of use that metal complexes of these ligands already find in homogeneous catalysis, they are likely to find wide usage in the future as photosensitizes and imaging agents.

## Experimental Section

### General Procedures, Materials and Instrumentation

$AuCl(SMe_2)$,[13] **[L1]I/BF$_4$**,[14] **[L2](BF$_4$)$_2$**[2g,15] and **1**[10] were prepared as described previously in the literature. Commercially available chemicals were used as purchased, unless otherwise noted. The solvents used for metal complex synthesis and cyclic voltammetry measurements were dried and distilled under nitrogen and degassed by common techniques prior to use. Column chromatography was performed over Silica 60 M (0.04 – 0.063 mm) or Aluminium oxide, neutral 60A (50-200μm). $^1$H and $^{13}$C{$^1$H} NMR spectra were recorded on a Jeol ECS 400 spectrometer. Chemical shifts are reported in ppm with reference to the residual solvent peaks. Multiplets are reported as follows: singlet (s), duplet (d), triplet (t) quartet (q), quintet (quint), and combinations thereof. Mass spectrometry was performed on an Agilent 6210 ESI-TOF.

### Single Crystal X-Ray Diffraction

X-Ray data were collected on a Bruker Smart AXS or Bruker D8 Venture system. Data were collected at 140(2) K using graphite-monochromated Mo K$\alpha$ radiation ($\lambda_\alpha$ = 0.71069 Å). The strategy for the data collection was evaluated by using the Smart software. The data were collected by the standard '$\omega$ scan techniques' and were scaled and reduced using Saint+ and SADABS software. The structures were solved by direct methods using SHELXS-97 or SHELXS_2014/7 and refined by full matrix least-squares, refining on $F^2$. Non-hydrogen atoms were refined anisotropically.[16] If it is noted, bond length and angles were measured with Diamond Crystal and Molecular Structure Visualization Version 3.1. CCDC 1015503 and 1015502 contain the cif files for this work.

**Electrochemistry**

Cyclic voltammograms were recorded with a PAR VersaStat 4 potentiostat (Ametek) with a conventional three-electrode configuration consisting of a carbon working electrode, a platinum auxiliary electrode and an Ag/AgCl reference electrode. The scan rate for each measurement is 100mV/s. The experiments were carried out in absolute THF containing 0.1 M $Bu_4NPF_6$ (dried, Fluka, ≥99.0 %, electrochemical grade) as the supporting electrolyte and at room temperature, unless otherwise noted.

**UV-vis and Emission Spectroscopy**

UV-vis spectra were recorded with an Avantes spectrometer consisting of a light source (AvaLight-DH-S-Bal), and UV-vis detector (AvaSpec-ULS2048), and a NIR detector (AvaSpec-NIR256-TEC). The UV/Vis absorption spectra were recorded on a Varian Cary 50 bio UV/Visible spectrophotometer in dichloromethane (DCM) solvent. Excitation and emission spectra were recorded in DCM on a FluoroMax®-4 spectrofluorimeter. Since emission spectra were obtained under 270 nm excitation, to record the spectra between 450 nm and 800 nm a filter with transmission >370 nm was used. Solutions were degassed using freeze pump thaw technique.

Lifetimes were recorded in both aerated and degassed solutions using an Edinburgh instruments mini-τ fluorescence lifetime spectrometer. Excitation was with a 270 nm ( ±10 nm) EPLED-270 with a 750 ps pulse width.

**DFT Calculations**

DFT calculations were done with the ORCA 3.0.0 program[17] package using the BP86 and B3LYP functional for the geometry optimization and single-point calculations respectively.[18] All calculations were run with empirical Van der Waals correction (D3).[19] Convergence criteria were set to default for the geometry-optimizations (OPT) and tight for SCF calculations (TIGHTSCF). Relativistic effects were included with the zeroth-order relativistic approximation (ZORA)[20]. Triple-ζ-valence basis sets (def2-TZVP)[21] were employed for all atoms. Calculations were performed using the resolution of the identity approximation[22] with matching auxiliary basis sets. Low-lying excitation energies were calculated with time-dependent DFT (TD-DFT). Solvent effects were taken into account with the conductor-like screening model (COSMO).[23] Spin densities were calculated according to the Löwdin

population analysis.[24] Molecular orbitals and spin densities were visualized with the Molekel 5.4.0.8 program.[25]

**Preparation of the Gold Carbene Complex [2]$BF_4$**

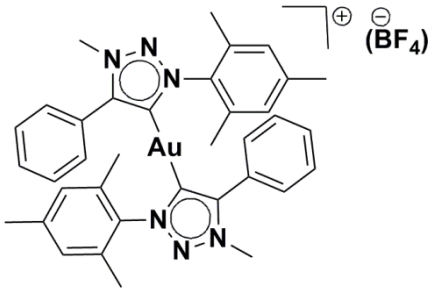


A mixture of complex **1** (1 equiv., 76.36 mg, 0.15 mmol) and silver(I)tetrafluoroborate (1 equiv., 29.20 mg, 0.15 mmol) was stirred in absolute dichloromethane (15 mL) at room temperature for 17 h under exclusion of light. The reaction mixture was filtered over Celite, washed with dichloromethane and the solvent was evaporated. The residue was re-resolved in dichloromethane (2mL) and precipitated with pentane (50 mL). The precipitate was collected by filtration. Complex **[2]$BF_4$** was obtained as a white solid in a yield of 40% (44.73 mg, 0.06 mmol) (based on gold 40%, based on the ligand 80%). Single crystals suitable for X-ray diffraction analysis were obtained by condensing hexane onto a concentrated solution of the complex in dichloromethane at room temperature.

$^1$H NMR (400 MHz, $CD_2Cl_2$, 25 °C) δ 7.62 – 7.52 (m, 6H, Aryl-*H*), 7.50 – 7.45 (m, 4H, Aryl-*H*), 6.94 (s, 4H, Aryl-*H*), 4.18 (s, 6H, 2xN-C*H*$_3$), 2.44 (s, 6H, 2xC*H*$_3$), 1.83 (s, 12H, 4xC*H*$_3$). $^{13}$C{$^1$H} NMR (101 MHz, 400 MHz, $CD_2Cl_2$, 25 °C) δ 174.3 (Carbene-*C*), 148.8, 141.0, 136.0, 134.7, 130.9, 129.9, 129.7, 129.6, 126.6 (all Aryl-*C*), 38.7 (N-*C*$H_3$), 21.6, 17.6 (all Alkyl-*C*). HRMS (ESI): calcd for [$C_{36}H_{38}AuN_6BF_4$] [$(M - BF_4)^+$] *m/z* 751.2823 found 751.2866.

**Preparation of the Gold Carbene Complex [3](BF$_4$)$_2$**

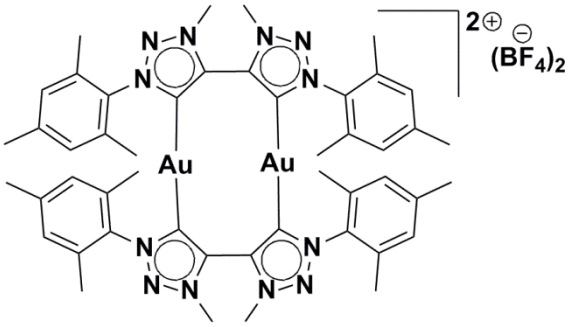


A mixture of [**L2](BF$_4$)$_2$** (1 equiv., 230.5 mg, 0.4 mmol) and silver(I)oxide (1 equiv., 92.7 mg, 0.4 mmol) was stirred in absolute acetonitrile (20 mL) at 50 °C for 24 h under exclusion of light. The reaction mixture was then filtered over Celite under $N_2$-atmosphere, washed with abs. acetonitrile and AuCl($SMe_2$) (0.95 equiv., 111.7 mg, 0.38 mmol) was added. After stirring the mixture for another 24 h at room temperature under exclusion of light, the reaction mixture was filtered over Celite, washed with acetonitrile and the solvent was evaporated. The residue was passed through a short pad of dry neutral aluminium oxide, eluted with dry acetonitrile and the solvent was evaporated. Addition of dichloromethane gives a white solid which was filtered and washed with pentane. Some of the product is still soluble in dichloromethane. For this the filtrate was reduced to 3 mL and precipitated with pentane, which gave a small but second amount of the product as a white solid. The yield of complex [**3](BF$_4$)$_2$** overall was 27% (148.79 mg, 0.108 mmol). Single crystals suitable for X-ray diffraction analysis were obtained by condensing diethyl ether onto a concentrated solution of the complex in acetonitrile at 8°C.

$^1$H NMR (400 MHz, $CD_3CN$, 25 °C) δ 7.11 (s, 4H, Aryl-*H*), 7.03 (s, 4H, Aryl-*H*), 4.33 (s, 12H, 4xN-C*H*$_3$), 2.36 (s, 12H, 4xC*H*$_3$), 1.88 (s, 12H, 4xC*H*$_3$), 1.68 (s, 12H, 4xC*H*$_3$). $^{13}$C{$^1$H} NMR (101 MHz, $CD_3CN$, 25 °C) δ 176.4 (Carbene-*C*), 142.2, 137.7, 136.1, 135.8, 135.3, 130.2, 130.0 (all Aryl-*C*), 41.1 (N-*C*H$_3$), 21.1, 17.6 (all Alkyl-*C*). HRMS (ESI): calcd for [$C_{48}H_{55}Au_2N_{12}B_2F_8$] [((M – 2BF$_4$)/2)$^+$] *m/z* 597.2036 found 597.2035.

**Acknowledgements**

We are grateful to the Deutsche Forschungsgemeinschaft (DFG) and the Fonds der Chemischen Industrie (FCI, doctoral stipend for S. K.) for the financial support of this project, and to the University of Sheffield and EPSRC (UK).

## References


[1] a) O. Schuster, L. Yang, H. G. Raubenheimer, M. Albrecht, *Chem. Rev.* **2009**, *109*, 3445–3478; b) R. H. Crabtree, *Coord. Chem. Rev.* **2013**, *257*, 755–766.

[2] a) J. D. Crowley, A.-L. Lee, K. J. Kilpin, *Aust. J. Chem.* **2011**, *64*, 1118–1132; b) D. Schweinfurth, N. Deibel, F. Weisser, B. Sarkar, *Nachr. Chem.* **2011**, 937–941; c) K. F. Donnelly, A. Petronilho, M. Albrecht, *Chem. Commun.* **2013**, *49*, 1145–1159; d) J. M. Aizpurua, R. M. Fratila, Z. Monasterio, N. Pérez-Esnaola, E. Andreieff, A. Irastorza, M. Sagartzazu-Aizpurua, *New J. Chem.* **2014**, *38*, 474–480; e) B. Schulze, U. S. Schubert, *Chem. Soc. Rev.* **2014**, *43*, 2522–2571; f) P. Mathew, A. Neels, M. Albrecht, *J. Am. Chem. Soc.* **2008**, *130*, 13534–13535; g) G. Guisado-Barrios, J. Bouffard, B. Donnadieu, G. Bertrand, *Organometallics*, **2011**, *30*, 6017-6021.

[3] a) R. Huisgen, R. Knorr, L. Möbius, G. Szeimies, *Chem. Ber.* **1965**, *98*, 4014–4021; b) R. Huisgen, G. Szeimies, L. Möbius, *Chem. Ber.* **1967**, *100*, 2494–2507; c) H. C. Kolb, M. G. Finn, K. B. Sharpless, *Angew. Chem. Int. Ed.* **2001**, *40*, 2004–2021; d) V. V. Rostovtsev, L. G. Green, V. V. Fokin, K. B. Sharpless, *Angew. Chem. Int. Ed.* **2002**, *41*, 2596–2599; e) C. W. Tornøe, C. Christensen, M. Meldal, *J. Org. Chem.* **2002**, *67*, 3057–3064.

[4] for selected examples see: a) R. Saravanakumar, V. Ramkumar, S. Sankararaman, *Organometallics* **2011**, *30*, 1689–1694; b) R. Maity, S. Hohloch, C. Y. Su, M. van der Meer, B. Sarkar, *Chem. Eur. J.* **2014**, *20*, 9952–9961; c) A. Petronilho, M. Rahman, J. A. Woods, H. Al-Sayyed, H. Müller-Bunz, J. M. Don MacElroy, S. Bernhard, M. Albrecht, *Dalton Trans.* **2012**, *41*, 13074–13080; d) E. C. Keske, O. V. Zenkina, R. Wang, C. M. Crudden, *Organometallics*, **2012**, *31*, 456–461; e) S. Hohloch, C.-Y. Su, B. Sarkar, *Eur. J. Inorg. Chem.* **2011**, 3067–3075; f) K. J. Kilpin, U. S. Paul, A. L. Lee, J. D. Crowley, *Chem. Commun.* **2011**, *47*, 328–330; g) T. Nakamura, T. Terashima, K. Ogata, S.-i. Fukuzawa, *Org. Lett.* **2011**, *13*, 620–623; h) M. Gazvoda, M. Virant, A. Pevec, D. Urankar, A. Bolje, M. Kocevar, J. Kosmrlj, *Chem. Commun.* **2016**, *52*, 1571-1574; i) S. Hohloch, B. Sarkar, L. Nauton, F. Cisnetti, A. Gautier, *Tetrahedron Lett.* **2013**, *54*, 1808–1812; j) R. Maity, A. Verma, M. van der Meer, S. Hohloch, B. Sarkar, *Eur. J. Inorg. Chem.* **2016**, 111–117; k) C. Mejuto, B. Royo, G. Guisado-Barrios, E. Peris, *Beilstein J. Org. Chem.* **2015**, *11*, 2584-2590; l) I. Strydom, G. Guisado-Barrios, I. Fernández, D. C. Liles, E. Peris, D. L. Bezuidenhout, *Chem. Eur. J.* **2017**, DOI: 10.1002/chem.201604567.

[5] a) R. Maity, A. Mekic, M. van der Meer, A. Verma, B. Sarkar, *Chem. Commun*. **2015**, *51*, 15106-15109; b) C. Mejuto, G. Guisado-Barrios, D. Gusev, E. Peris, *Chem. Commun.* **2015**, *51*, 13914–13917; c) R. Maity, M. van der Meer, S. Hohloch and B. Sarkar, *Organometallics*, **2015**, *34*, 3090-3096; d) R. Maity, T. Tichter, M. van der Meer, B. Sarkar, *Dalton Trans*. **2015**, *44*, 18311-18315.

[6] a) V. Leigh, W. Ghattas, R. Lalrempuia, H. Müller-Bunz, M. T. Pryce, M. Albrecht, *Inorg. Chem.* **2013**, *52*, 5395–5402; b) S. Sinn, B. Schulze, C. Friebe, D. G. Brown, M. Jager, E. Altuntas, J. Kubel, O. Guntner, C. P. Berlinguette, B. Dietzek, U. S. Schubert, *Inorg. Chem.* **2014**, *53*, 2083–2095; c) Y. Liu, K. S. Kjaer, L. A. Fredin, P. Chabera, T. Harlang, S. E. Canton, S. Lidin, J. Zhang, R. Lomoth, K. E. Bergquist, P. Persson, K. Warnmark, V. Sundstrom, *Chem. Eur. J.* **2015**, *21*, 3628–3639; d) A. R. Naziruddin, C. S. Lee, W. J. Lin, B. J. Sun, K. H. Chao, A. H. Chang, W. S. Hwang, *Dalton Trans.* **2016**, *45*, 5848–5859; e) J. Soellner, M. Tenne, G. Wagenblast, T. Strassner, *Chem. Eur. J.* **2016**, *22*, 9914–9918; f) A. Baschieri, F. Monti, E. Matteucci, A. Mazzanti, A. Barbieri, N. Armaroli, L. Sambri, *Inorg. Chem*. **2016**, *55*, 7912-7919.

[7] a) M. van der Meer, E. Glais, I. Siewert and B. Sarkar, *Angew. Chem. Int. Ed.* **2015**, *54*, 13792–13795; b) L. Hettmanczyk, S. Manck, C. Hoyer, S. Hohloch, B. Sarkar, *Chem. Commun.* **2015**, *51*, 10949–10952; c) L. Hettmanczyk, L. Suntrup, S. Klenk, C. Hoyer, B. Sarkar, *Chem. Eur. J*. **2017**, *23*, 576-585; d) R. Maity, M. van der Meer, B. Sarkar, *Dalton Trans*. **2015**, *44*, 46-49.

[8] a) D. Canseco-Gonzalez, A. Petronilho, H. Müller-Bunz, K. Ohmatsu, T. Ooi, M. Albrecht, *J. Am. Chem. Soc.* **2013**, *135*, 13193–13203; b) L.-A. Schaper, X. Wei, S. J. Hock, A. Pöthig, K. Öfele, M. Cokoja, W. A. Herrmann and F. E. Kühn, *Organometallics* **2013**, *32*, 3376–3384; c) J. R. Wright, P. C. Young, N. T. Lucas, A. L. Lee, J. D. Crowley, *Organometallics* **2013**, *32*, 7065–7076; d) D. Mendoza-Espinosa, R. González-Olvera, G. E. Negrón-Silva, D. Angeles-Beltrán, O. R. Suárez-Castillo, A. Álvarez-Hernández, R. Santillan, *Organometallics* **2015**, *34*, 4529–4542; e) D. Mendoza-Espinosa, R. González-Olvera, C. Osornio, G. E. Negrón-Silva and R. Santillan, *New J. Chem.* **2015**, *39*, 1587–1591; f) D. R. Tolentino, M. Liqun Jin and G. Bertrand, *Chem. Asian J.* **2015**, *10*, 2139–2142; g) R. Pretorius, M. R. Fructos, H. Müller-Bunz, R. A. Gossage, P. J. Perez, M. Albrecht, *Dalton Trans.* **2016**, *45*, 14591; *h*) M. Frutos, M. A. Avello, A. Viso, R. F. de la Pradilla, M. C. de la Torre, M. A. Sierra, H. Gornitzka, C. Hemmert, *Org. Lett.* **2016**, *18*, 3570-3573; i) L. Hettmanczyk, D. Schulze, L. Suntrup, B. Sarkar, *Organometallics*, **2016**, *35*, 3828-3836.

[9] For selected examples see: a) V. J. Catalano, A. L. Moore, *Inorg. Chem.* **2005**, *44*, 6558−6566; b) P. J. Barnard, L. E. Wedlock, M. V. Baker, S. J. Berners-Price, D. A. Joyce, B. W. Skelton, J. H. Steer, *Angew. Chem. Int. Ed.* **2006**, *45*, 5966–5970; c) L. Ray, M. M. Shaikh, P. Ghosh, *Inorg. Chem.* **2008**, *47*, 230–240; d) V. W. Yam, E. C. Cheng, *Chem. Soc. Rev.* **2008**, *37*, 1806-1813; e) J. C. Y. Lin, R. T. W. Huang, C. S. Lee, A. Bhattacharyya, W. S. Hwang, I. J. B. Lin, *Chem. Rev.* **2009**, *109*, 3561–3598; f) J. Gil-Rubio, V. Cámara, D. Bautista, J. Vicente, *Organometallics* **2012**, *31*, 5414–5426; g) M. Kriechbaum, G. Winterleitner, A. Gerisch, M. List, U. Monkowius, *Eur. J. Inorg. Chem.* **2013**, 5567–5575; h) C. Tubaro, M. Baron, M. Costante, M. Basato, A. Biffis, A. Gennaro, A. A. Isse, C. Graiff, G. Accorsi, *Dalton Trans.* **2013**, *42*, 10952–10963; i) R. Visbal, I. Ospino, J. M. Lopez-de-Luzuriaga, A. Laguna, M. C. Gimeno, *J. Am. Chem. Soc.* **2013**, *135*, 4712–4715; j) F. F. Hung, W. P. To, J. J. Zhang, C. Ma, W. Y. Wong, C. M. Che, *Chem. Eur. J.* **2014**, *20*, 8604–8614; k) S. Bestgen, M. T. Gamer, S. Lebedkin, M. M. Kappes, P. W. Roesky, *Chem. Eur. J.* **2015**, *21*, 601-614; l) R. Visbal, M. C. Gimeno, *Chem. Soc. Rev.* **2014**, *43*, 3551-3574.

[10] M. Rigo, L. Hettmancyzk, F. J. L. Heutz, S. Hohloch, M. Lutz, B. Sarkar, C. Müller, *Dalton Trans.* **2017**, *46*, 86-95.

[11] A. Bondi, *J. Phys. Chem.* **1964**, *68*, 441–451.

[12] a) D. S. Weinberger, N. Amin Sk, K. C. Mondal, M. Melaimi, G. Bertrand, A. C. Stuckl, H. W. Roesky, B. Dittrich, S. Demeshko, B. Schwederski, W. Kaim, P. Jerabek, G. Frenking, *J. Am. Chem. Soc.* **2014**, *136*, 6235–6238; b) D. S. Weinberger, M. Melaimi, C. E. Moore, A. L. Rheingold, G. Frenking, P. Jerabek, G. Bertrand, *Angew. Chem. Int. Ed.* **2013**, *52*, 8964–8967.

[13] T. N. Hooper, C. P. Butts, M. Green, M. F. Haddow, J. E. McGrady, C. A. Russell, *Chem. Eur. J.* **2009**, *15*, 12196–12200.

[14] J. E. M. N. Klein, M. S. Holzwarth, S. Hohloch, B. Sarkar, B. Plietker, *Eur. J. Org. Chem.* **2013**, 6310–6316.

[15] S. Hohloch, L. Suntrup, B. Sarkar, *Inorg. Chem. Front.* **2016**, *3*, 67–77.

[16] a) . M. Sheldrick, *SHELXS-97, Program for Crystal Structure Solution and Refinement*, University of Göttingen: Göttingen, Germany, **1997**; b) SAINT+, *Data Integration Engine, Version 8.27b©*, Bruker AXS Inc., Madison, Wisconsin, USA, **1997–2012**; c) G. M. Sheldrick, *Acta Cryst.* **2008**, *64*, 112–122; d) Bruker, *APEX2*, Bruker AXS Inc., Madison, Wisconsin, USA, **2012**; e) G. M. Sheldrick, *SHELXL Version 2014/7, Program for crystal structure solution and refinement*, University of Göttingen:

Göttingen, Germany, **2014**; f) G. M. Sheldrick, *Acta Cryst.* **2015**, *71*, 3–8; g) G. M. Sheldrick, *SADABS. Program for Empirical Absorption Correction.*, University of Gottingen: Göttingen Germany, **SADABS Ver. 2008/1**.

[17] F. Neese, *WIREs Comput Mol Sci* **2012**, *2*, 73–78.

[18] a) A. D. Becke, *J. Chem. Phys.* **1993**, *98*, 5648; b) A. D. Becke, *Phys. Rev. A* **1988**, *38*, 3098–3100; c) C. Lee, W. Yang, R. G. Parr, *Phys. Rev. B* **1988**, *37*, 785–789.

[19] S. Grimme, J. Antony, S. Ehrlich, H. Krieg, *J. Chem. Phys.* **2010**, *132*, 154104.

[20] C. van Wüllen, *J. Chem. Phys.* **1998**, *109*, 392.

[21] F. Weigend, R. Ahlrichs, *Phys. Chem. Chem. Phys*. **2005**, *7*, 3297.

[22] a) F. Neese, *J. Comput. Chem.* **2003**, *24*, 1740–1747; b) F. Neese, F. Wennmohs, A. Hansen, U. Becker, *Chem. Phys.* **2009**, *356*, 98–109; c) O. Vahtras, J. Almlöf, M. W. Feyereisen, *Chem. Phys. Lett.* **1993**, *213*, 514–518; d) J. L. Whitten, *J. Chem. Phys.* **1973**, *58*, 4496.

[23] a) A. Klamt, G. Schüürmann, *J. Chem. Soc., Perkin Trans. 2* **1993**, 799; b) S. Sinnecker, A. Rajendran, A. Klamt, M. Diedenhofen, F. Neese, *J. Phys. Chem. A* **2006**, *110*, 2235–2245.

[24] P.-O. Löwdin, *J. Chem. Phys.* **1950**, *18*, 365.

[25] S. Portmann, Molekel, version 5.4.0.8; CSCS/UNI, Geneva, Switzerland, **2009**.

TOC

Mono and dinuclear gold(I) complexes display triazolylidene based reduction and display excited state lifetimes of several microseconds.